FAULT SCALING ON MARS: SLIP DISTRIBUTION AND DISPLACEMENT-LENGTH RELATIONSHIP DERIVED FROM HRSC DATA.

E. Hauber[1], T. Jonas[1], M. Voelker[1], M. Knapmeyer[1], M. Grott[1], K.-D. Matz[1], Institut für Planetenforschung, DLR, Berlin, Germany (Ernst.Hauber@dlr.de).

Summary: We determined the slip distribution along normal faults on Mars, using Digital Elevation Models (DEM) and corresponding orthoimages derived from High Resolution Stereo Camera (HRSC) data. The fault scaling values (i.e. D_{max}/L; Fig. 1) of unlinked fault segments display a large scatter and follow a relationship of $D_{max} \approx 0.008 \cdot L$. If fault segment linkage is considered, the D_{max}/L ratio slightly decreases ($D_{max} \approx 0.006 \cdot L$). Our results are consistent with results for terrestrial faults, but show a slightly higher D_{max}/L ratio than previous studies of planetary faults. We ascribe this to our use of high-resolution topographic data, because the location of D_{max} may be underestimated when using lower-resolution data.
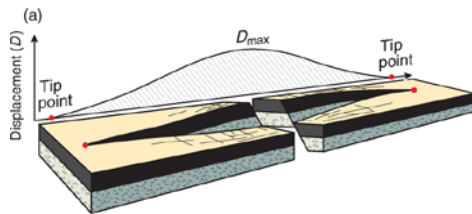
Figure 1. Schematic view of normal fault geometry, corresponding displacement profile, and terminology used in this study (from [1]).

Data and Methods: All measurements are based on HRSC DEM and orthoimages. Individual DEM have typical grid sizes of 50 to 100 m, corresponding orthoimages have resolutions of 12.5 to 25 m px^{-1}. For detailed structural interpretation of key locations (e.g., relay ramps), MOC and CTX images have been inspected where available. Fault length was digitized along the fault line, and multiple topographic cross-sections normal to fault trend were drawn with a spacing of ~1 km. Fault throw (a proxy for true displacement) was visually determined in the cross-sections.

Background and Motivation: Geometric fault properties can provide insights into the mechanical and temporal evolution of fault systems [2,3] and the past and future potential for seismic energy release [4]. In planetary science, where a lack of seismometers is unfortunately the rule rather than the exception, the analysis of faults with remote sensing data typically provides the only direct observational evidence to constrain the tectonic history of a planet [5]. Since the seismic moment released during the growth of a fault is strongly connected to the fault geometry, the study of fault populations can also help to estimate the current seismicity level [6,7]. Until today, however, only few data on the relationships between fault displacement and length have been collected for extraterrestrial bodies [8], partly due to the limited number of reliable topographic datasets. Here we use DEM and orthoimages from HRSC [9] to obtain information on the displacement distribution along fault traces. This also enabled determining the maximum displacement. We compare our results to previous measurements of faults on Mars, Earth, and other planets. Based on these analyses, we discuss the implications of fault segmentation and linkage for further interpretation.

Results: The locations of study areas were determined by the availability of HRSC DEM with high accuracy (Alba Mons (E flank), Tempe Terra, Ophir Planum, and Claritas and Tantalus Fossae). The most challenging aspect was the identification of individual faults or fault segments with little evidence for degradation and cross-cutting relationships with other faults. Fault growth by segment linkage clearly appears to be an important process in the evolution of Martian fault populations (Fig. 2), and faults were considered to be linked when relay ramps were observed (Fig. 2 and 4); We applied the linkage criterion of ref. [10]. The length range of faults for which the displacement could be determined spans about 1.5 orders of magnitude (Fig. 3). So far, no faults shorter than a few km could be reliably measured. The D/L ratio is in the order of 10^{-2} (0.006; Figs. 3 and 4), consistent with values determined for terrestrial faults (Fig. 5) [11].

Conclusion: Our preliminary results show that the displacement profiles of normal faults on Mars bear information on fault evolution by segment linkage (see also [12]). The D_{max}/L ratio is roughly centered at a value of 10^{-2}, which is also observed for terrestrial faults, but slightly higher than some previous estimates for planetary D_{max}/L ratios (Fig. 3). This may result from improved D_{max} determination in highly resolved DEM. Our data display a large scatter, and we found it difficult to measure faults shorter than ~5 km. This may attributed to the fact that Martian faults are rarely observed in bedrock and, therefore, small faults would appear "blurred" in regolith. Extension of our approach to bedrock (e.g., layered deposits in Valles Marineris) might mitigate this problem and extend the length range of analyzed faults.
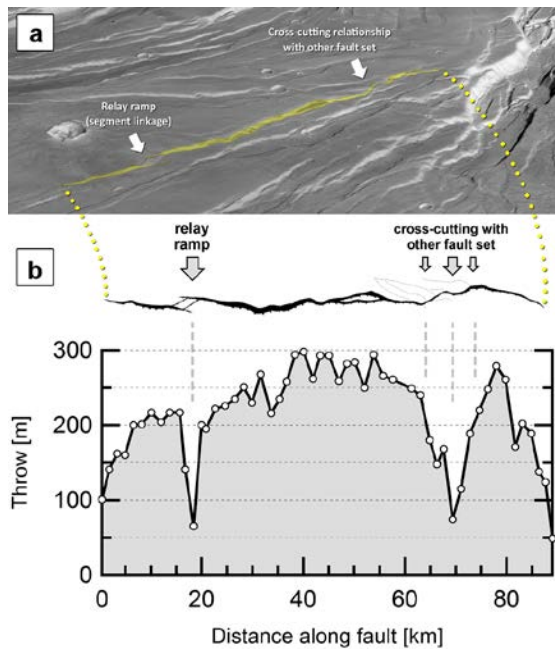
Figure 2: Example of normal fault on Mars and corresponding displacement profile. (a) Perspective 3D-view of normal faults in Tempe Terra, Mars (center at 39.13°N/285.89°E, view is toward N, sun from right). Note many relay ramps linking fault segments. The fault shown in the lower panel is highlighted in yellow (image width ~ 110 km). (b) Mapped normal fault in plan view *(top)* and associated slip distribution *(bottom)*. Note that distinct minima are associated with a relay ramp (left) and a location where the fault is cross-cut by another fault set (right). This example shows that the excellent preservation of fault morphology on Mars due to the small erosion rates enables interpreting displacement profiles in detail.
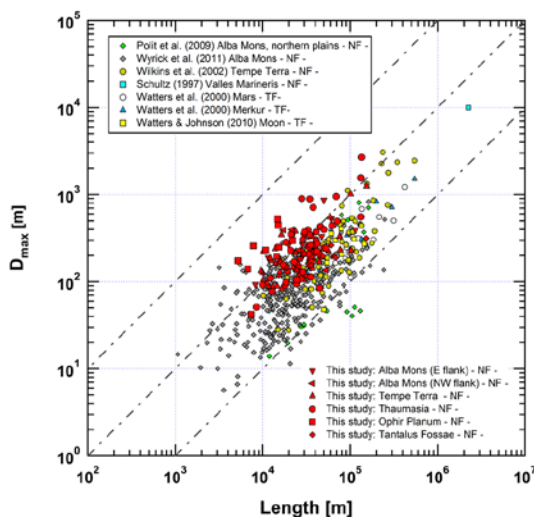
Figure 3. D_{max} vs. L for unlinked normal faults measured in this study (red symbols). D_{max} /L values for other planetary fault are plotted for comparison (NF-normal faults, TF-thrust faults).
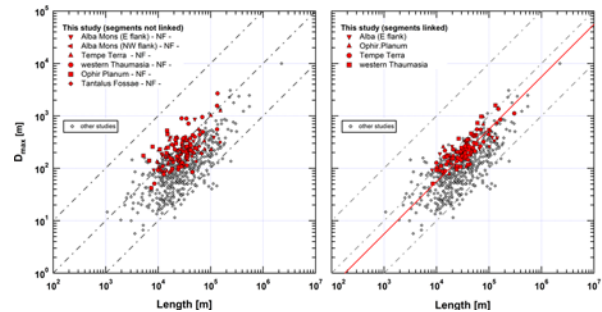
Figure 4. Effect of fault linkage on D_{max} /L ratio. *(left)* D_{max} vs. L for unlinked normal faults measured in this study (same as Fig. 3; grey symbols for other planetary faults). *(right)* D_{max} vs. L for normal faults after segment linkage. Note that segment linkage appears to slightly decrease D_{max} and decreases the scatter of the data (i.e. the point cloud becomes more "linear"). Red line represents best linear fit to the data ($\gamma = 0.006$).
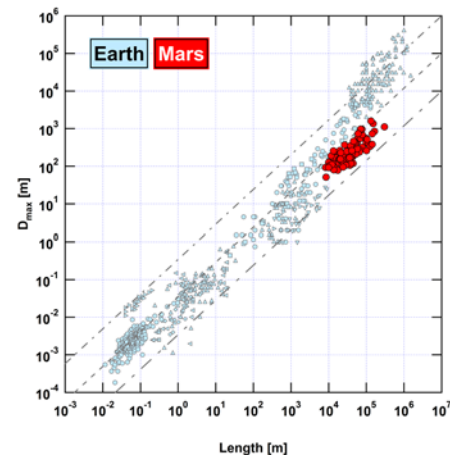
Figure 5. D_{max} /L values as determined in this study for linked faults (red symbols, same as in right part of Fig. 4) in comparison to published values for terrestrial faults (light blue symbols; from refs. [12,13] and other sources).

References: [1] Fossen, H. (2010) *Structural Geology*, Cambridge Univ. Press. [2] Cartwright, J.A. et al. (1995) *J. Struct. Geol.,* 17, 1319-1326. [3] Cowie, P.A. and Scholz, C.H. (1992) *J. Struct. Geol.,* 14, 1133-1148. [4] Wells, D.L. and Coppersmith, K.J. (1994) *Bull. Seismol. Soc. Amer.,* 84, 974-1002. [5] Schultz, R.A. et al. (2010) *J. Struct. Geol.,* 32, 855-875. [6] Golombek, M.P. et al. (1992) *Science* 258, 979-981. [7] Knapmeyer, M. et al. (2006) *J. Geophys. Res.,* 111, E11006. [8] Schultz, R.A. et al. (2006) *J. Struct. Geol.,* 28, 2182-2193. [9] Gwinner, K. et al. (2010) *Earth Planet. Sci. Lett.,* 294, 506-519. [10] Soliva, R. and Benedicto, A. (2004) *J. Struct. Geol.,* 26, 2251-2267. [11] Scholz, C.H. (1997) *Int. J. Rock Mech. & Min. Sci.,* 34(3-4), Paper No. 273, 1997. [12] Wyrick, D.Y., et al. (2011) *Icarus, 212,* 559-567. [13] Schlische, R.W. et al. (1996) *Geology, 24,* 683-686.